Satellite-Based Insights into Precipitation Formation Processes in Continental and Maritime Convective Clouds

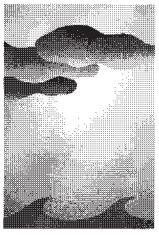

Daniel Rosenfeld and Itamar M. Lensky
Institute of Earth Sciences, Hebrew University of Jerusalem, Jerusalem, Israel

ABSTRACT

Multispectral analyses of satellite images are used to calculate the evolution of the effective radius of convective cloud particles with temperature, and to infer from that information about precipitation forming processes in the clouds. Different microphysical processes are identified at different heights. From cloud base to top, the microphysical classification includes zones of diffusional droplet growth, coalescence droplet growth, rainout, mixed-phase precipitation, and glaciation. Not all zones need appear in a given cloud system. Application to maritime clouds shows, from base to top, zones of coalescence, rainout, a shallow mixed-phase region, and glaciation starting at −10°C or even warmer. In contrast, continental clouds have a deep diffusional growth zone above their bases, followed by coalescence and mixed-phase zones, and glaciation at −15° to −20°C. Highly continental clouds have a narrow or no coalescence zone, a deep mixed-phase zone, and glaciation occurring between −20° and −30°C. Limited aircraft validation for the satellite inferences over Israel, Thailand, and Indonesia is available.

Substantial transformation in the microphysical and precipitation forming processes is observed by this method in convective clouds developing in air masses moving from the sea inland. These changes appear to be related to the modification of the maritime air mass as it moves inland and becomes more continental. Further transformations are observed in air masses moving into areas affected by biomass burning smoke or urban air pollution, such that coalescence, and thus precipitation, is suppressed even in deep tropical clouds. It follows that natural and anthropogenic aerosols can substantially modify clouds not only in pristine environments, as was already demonstrated by the ship tracks, but they can also incur profound impact on cloud microstructure and precipitation in more continental environments, leading to substantial weather modification in densely populated areas.

1. Introduction

About 10 years ago, with the newly acquired capabilities of remote sensing from space, tracks of enhanced cloud reflectivity over the open ocean became widely recognized as the impact of ship-stack effluent on the cloud drop size distribution and water content (Coakley et al. 1987; Radke et al. 1989). These ship tracks provided a vivid demonstration of the profound effect of anthropogenic aerosols on the radiative properties and microphysical structure of maritime stratocumulus clouds. Despite these new insights, the understanding of the effects of aerosols on cloud radiative and precipitation properties is still limited. Moreover, the effects of those aerosols and their feedback mechanisms are recognized as a major source of uncertainty in the current assessment of global climate change (Houghton et al. 1994).

Platnick and Twomey (1994) have shown that the sensitivity of cloud visible albedo to changes in drop size distribution is greatest for shallow clouds, because very thick and water-rich clouds have large visible albedoes, regardless of their drop sizes. However, according to the satellite observations reported here, the precipitation formation processes are sensitive to aerosols regardless of cloud depth. These observations are based on analyses of the relationships between

Corresponding author address: Dr. Daniel Rosenfeld, Institute of Earth Sciences, Hebrew University of Jerusalem, 91904 Jerusalem, Israel.
E-mail: daniel@vms.huji.ac.il
In final form 7 May 1998.

satellite-retrieved effective radius (r_e) and the cloud-top temperature (T) of convective clouds growing in maritime, transition, and continental air masses. The terms "continental" and "maritime" clouds are used hereafter in their microphysical connotation; that is, continental clouds are composed of many small drops, while the maritime clouds have small concentrations of larger droplets.

The observations show large variability in the cloud microstructure that is consistent with the suggestion that airmass properties have a profound impact on precipitation formation processes in convective clouds, including deep cumulonimbus convection.

The objectives of this paper are the following.

- Presentation of a methodology by which precipitation formation processes can be inferred from the satellite data, using both a color visualization scheme and a computerized algorithm for identification of different microphysical processes at different distances above cloud base.
- Validation of the methodology by in situ aircraft measurements.
- Presentation of preliminary results linking various inferred microphysical processes to the airmass properties (i.e., continental vs maritime).

The next section describes a qualitative cloud microphysical classification. The effective radius is used as an indicator of precipitation and a visualization scheme is presented. Physical arguments are provided for the analysis of the relationships between temperature and effective radius for convective clouds as the basis for a quantitative cloud microphysical classification. Case studies are presented in section 3 and a description of the quantitative cloud microphysical classification scheme follows in section 4. This classification is applied to additional, more complex case studies in section 5. In situ aircraft validation is provided in section 6. Finally, a discussion of the classification scheme and the significance of the insights gained by it is given in section 7.

2. Cloud-top multispectral classification

a. The effective radius

A new way to use standard operational satellite data for deducing the structure of clouds and their precipitation formation processes is presented. It is based on display and analyses of the Advanced Very High Resolution Radiometer (AVHRR) data from the National Oceanic and Atmospheric Administration (NOAA) operational weather satellites, which provide subsatellite 1.1-km data at five channels centered at 0.65, 0.9, 3.7, 10.8, and 12.0 μm. A key parameter in the inferences is the retrieved, effective, cloud-top particle radius, as defined by

$$r_e = \frac{\int_0^\infty r^3 n(r)\,dr}{\int_0^\infty r^2 n(r)\,dr}, \tag{1}$$

where $n(r)$ is the number concentration of particles having radius r.

The effective radius of fully cloudy pixels is calculated using an inversion of a radiative transfer model (Nakajima and King 1990), with the mid-IR (3.7 μm) cloud reflectance ($\rho_{3.7}$) and the viewing geometry as inputs. The quantitative analysis is done only on clouds thick enough to be potential precipitation producers. Cloudy pixels were identified as pixels with

- visible reflectance (0.65 μm) greater than 0.4, and
- brightness temperature difference—BTD (channels 4 and 5) smaller than

$$\mathrm{BTD}_S(T) + 1°\mathrm{C},$$

where subscript s stands for saturation. The precipitable water of a saturated atmosphere $\mathrm{PW}_S(T)$ above the isotherm T was calculated, and Eq. (2) from Eck and Holben (1994) for Mali, West Africa, was used to get $\mathrm{BTD}_S(T)$:

$$\mathrm{PW} = 0.837\ \mathrm{BTD}. \tag{2}$$

The cloud reflectance in mid-IR was computed assuming that the emissivity of clouds in the IR (11 μm) is equal to 1.0, and that the transmission through a cloud in the 3.7-μm channel is zero.

Following Kaufman and Nakajima (1993), the top-of-the-atmosphere radiance at 3.7 ($L_{3.7}$) and 11 μm (L_{11}) is

$$L_{3.7} = t_{3.7}^0\left(\frac{F_0\mu_0}{\pi}\right)\rho_{3.7} + t'_{3.7}B_{3.7}(T)\left(1-\rho_{3.7}\right), \tag{3}$$

$$L_{11} = t'_{11}B_{11}(T), \tag{4}$$

where $t^0_{3.7}$ is the total downward and then upward transmission of sunlight above the cloud at the 3.7-μm channel; $t'_{3.7}$ and t'_{11} are the upward transmissions above the cloud at the 3.7- and 11-μm channels, respectively; F_0 is the extraterrestrial solar flux in the 3.7-μm channel; μ_0 is the cosine of the solar zenith angle; and $B_i(T)$ is the Plank function for temperature T and wavelength i. The cloud reflectance can be derived from Eqs. (3) and (4):

$$\rho_{3.7} = \frac{L_{3.7} - t'_{3.7}B_{3.7}(T)}{\left(t^0_{3.7}F_0\mu_0/\pi\right) - \left[t'_{3.7}B_{3.7}(T)\right]}, \quad \text{where } T = B_{11}^{-1}\left(\frac{L_{11}}{t'_{11}}\right). \tag{5}$$

The transmission functions $t^0_{3.7}$, $t'_{3.7}$, and t'_{11} depend on the precipitable water above the cloud. The method was used on a wide range of atmospheric conditions, thus the following approximation was used for the calculation of $t^0_{3.7}$:

$$t^0_{3.7} = e^{-\left(\frac{\mathrm{PW}}{\mathrm{PW}_S}\frac{a_S}{\mu\mu_0}\right)}. \tag{6}$$

Here, PW was calculated using (2); PW_S and a_S = 0.4 are the precipitable water and the maximal absorption in saturated atmosphere above a cloud top of 20°C, respectively; and μ is the cosine of the satellite zenith angle. The transmissions $t'_{3.7}$, and t'_{11} tend to balance each other in (5), therefore, we assume $t'_{3.7}$ = t'_{11} = 1. The retrieval is not very sensitive to the values of $t^0_{3.7}$.

The maximum value of the effective radius that can be retrieved by this method is 30 μm, because the 3.7-μm reflectance decreases to near the instrument noise level for clouds of larger particles. It has been shown (Rosenfeld and Gutman 1994) that an effective radius of 14 μm is a threshold value above which clouds contain precipitation size particles that can be detected by weather radars.

b. Visual multispectral classification scheme

An important step in the understanding of the complex interactions among cloud type, temperature, thickness, r_e, and the input aerosols is a clear visualization of these multiparameter data. This is facilitated by coding various combinations of visible reflectance, temperature and r_e as different colors, shown in the case studies according to the following scheme. 1) The visible reflectance modulates the red (brighter is redder); 2) the reflectance component at 3.7 μm, which is a surrogate for r_e in clouds, modulates the green (smaller r_e is greener); and 3) the 10.8-μm brightness temperature modulates the blue (warmer is bluer). Ice absorbs twice as much as water at 3.7 μm. Furthermore, ice particles are typically much larger than cloud droplets at the same temperature. Therefore, ice clouds or snow on the ground appear as having very large effective radius, or very low green in the color images. For the same reason, small effective radius indicates water clouds, even at temperatures below 0°C, where the cloud is said to be composed of supercooled water. Such clouds appear yellow in the color scheme.

A detailed color pallet relating the different color combinations to the numerical values of the three components is provided in appendix A. A corresponding cloud classification scheme is provided in appendix B.

c. The T *versus* r_e *relations for convective clouds*

The dependence of the effective radius on cloud-top temperature (T) for growing convective clouds can reveal the evolution of the particles composing the clouds and hence the various processes leading to the precipitation formation in them. The tops of convective cloud become colder with height in accordance with the nearby atmospheric sounding. Therefore, T can be used instead of cloud-top height to assess the vertical development of a cloud. Because a satellite image is a snapshot at an instant in time, analysis of clusters of convective clouds at different degrees of vertical development is done to infer the time evolution of the individual cloud elements. To do this, one must assume that cloud-top properties observed simultaneously for clouds at different stages of their vertical growth are similar to the properties of a single cloud as it grows through the various heights (Arakawa and Schubert 1974). In other words, cloud effective radius is a conserved property for a given temperature, as long as precipitation has not developed. The validity of this assumption is addressed in the section of the paper presenting aircraft validation of the satellite inferences (section 6).

A convective cloud can be described as one that ingests air mainly through its base and detrains at least some of that air through the cloud top (Arakawa and Schubert 1974). On that basis, it can be assumed that,

in a given convective cloud, the particle size increases monotonically from base to top, up to precipitation particle sizes, which fall from cloud top. This relationship of increasing r_e with height is often obscured by intervening nonconvective clouds. The particle sizes of thin layer clouds are typically much smaller than the particle sizes in the tops of convective clouds having much lower bases, which grow and penetrate these layer clouds. Observations of particle sizes can, therefore, be used to separate a mixture of layer and convective clouds (Lensky and Rosenfeld 1997). The T versus r_e relations were calculated for selected cloud clusters such that for each 1°C interval a distribution of r_e was obtained.

The actual composite is done in the following steps.

1) Define a window containing a convective cloud cluster with elements representing all growing stages, typically containing several thousands pixels.
2) Calculate the median and other percentiles of the r_e for each 1°C interval of cloud-top temperature (T).
3) Display graphically the T versus r_e curves of the 10th, 25th, 50th, 75th, and 90th percentiles.
4) Analyze the shape of the median (50th percentile) to find the microphysical zones, as defined in section 4.

The shape of the T versus r_e diagrams contains much information on the microphysical processes in the clouds. It is known that droplets grow mostly by diffusion at small distances above the bases of convective clouds, while higher up in the cloud the growth rate often accelerates by coalescence and ice processes. Because nearly all cloud droplets are nucleated at cloud base and cloud water mass increases less than linearly with depth, the increase in r_e in clouds under diffusional growth is proportional to D^a, where D is depth above cloud base, and the exponent a is at most 1/3. The power a would be 1/3 when the cloud water content increases linearly with decreasing T. In reality, the cloud water increases at a smaller rate, so that $a < 1/3$. Depth D can be approximated by $T_b - T$, where T_b is the cloud-base temperature (the warmest cloudy pixel + 2°C), and then $r_e \propto (T_b - T)^a$, where $a < 1/3$. A deviation from such a curve indicates the existence of mechanisms that amplify the particles' growth rate, such as coalescence and ice formation processes. These amplification processes are crucial to the formation of precipitation.

3. Case studies of maritime and continental clouds

Four case studies are provided in which airmass and cloud microphysical properties are related to each other in a systematic way. First, two "classic" cases of tropical clouds growing in pristine maritime clouds (central Indian Ocean) and in a highly polluted air mass (Sumatra engulfed by smoke from forest fires) are examined. The other two cases show clouds change their microstructure and precipitation-forming processes in air masses that move from sea inland, and further changes that occur in clouds forming over a major urban area.

a. Highly maritime clouds

The first case is of cumulus and cumulonimbus clouds (Fig. 1) growing in pristine maritime air over the central Indian Ocean, centered at 4°S and 80°E. The dominant red colors in Fig. 1 indicate large mid-IR absorption caused by the large cloud particles at all heights. The magenta color indicates large droplets already at warm temperatures or at small depth above cloud bases. This is shown quantitatively in Fig. 2, where r_e quickly grows with height and exceeds the precipitation threshold of 14 μm at the lowest observed levels, suggesting warm rain (i.e., rain formed by water drop coalescence) formation processes starting a short distance above cloud base. The r_e reaches a plateau of about 23 μm near the 13°C isotherm level, suggesting full development of warm rain processes at that level. Further increase of r_e at the supercooled levels indicates the formation of the ice phase. The maximum value of r_e, reached at −7°C, implies full development of the ice phase at that temperature. The warm glaciation temperature is consistent with the numerous aircraft observations of nearly complete glaciation of tropical maritime clouds at that temperature (Black and Hallett 1986; Jorgensen and LeMone 1989). This implies a much shallower mixed-phase zone compared to continental clouds, as described in the next section.

b. Highly continental clouds

At the other end of the cloud spectrum are observed tropical clouds growing in an air mass that is highly polluted by smoke emitted from the rain forest fires that occurred in Indonesia during October 1997. The smoke is visible in Fig. 3. Smoke from burning rain forests over the Amazon was documented by Kaufman and Farser (1997) as having particles with typical radius of 0.14 ± 0.02 μm, thus serving as source for nu-

merous small cloud condensation nuclei (CCN). Clouds forming in an air mass with such a CCN population are typically composed of many small droplets, and are thus considered microphysically highly continental. The coloration of the image of the clouds growing in the smoke-plagued air mass over Sumatra (Fig. 4, areas 1 and 2) suggests small water droplets at low levels (indicated in white), supercooled small drops higher up (indicated in yellow and light orange), and glaciated anvils, indicated in red. The T versus r_e curve in Figs. 5a and 5b show small r_e, well below the precipitation threshold of 14 μm to a temperature of about −10°C, indicating cloud droplet growth mainly by diffusional processes, without much coalescence. The r_e reaches a maximum near −22° to −25°C, implying full development of the ice phase at that temperature. Therefore, the clouds contain a deep mixed-phase zone and form the precipitation mainly in the ice phase as hail, graupel, and snow particles. The T versus r_e curves of the two cases (Fig. 2 and Figs. 5a,b) are consistent with the classic description of microphysically continental and maritime clouds, respectively (Squires 1958).

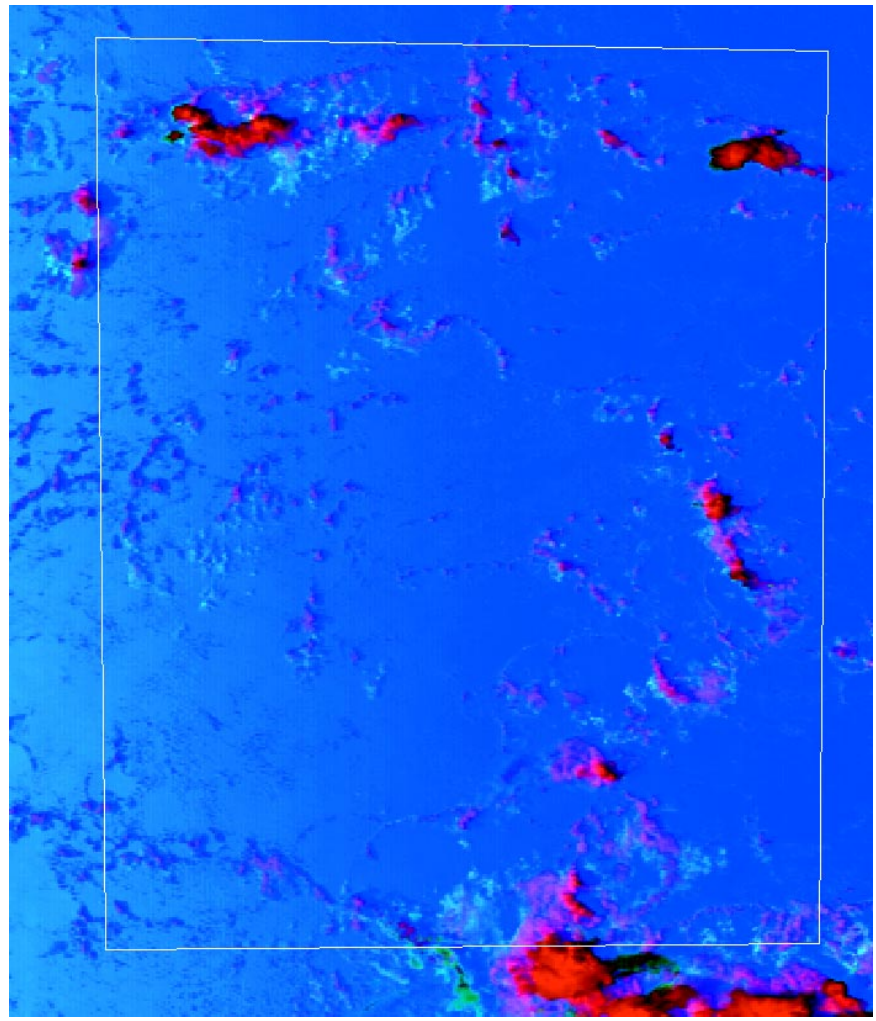

FIG. 1. A NOAA/AVHRR image from 9 December 1997 0900 UTC, of equatorial maritime clouds over the central Indian Ocean, in an area of 350 × 450 km, centered at 3°S, 80°E. North is at the top of the image. The color is composed of red for visible reflectance, green for 3.7-μm reflectance (approximating r_e), and blue for the inverse of 10.8-μm brightness temperature. The dominant magenta and red colors of the clouds indicate that they are composed of very large particles, thus highly maritime. A detailed color pallet is provided in appendix A. A cloud classification pertaining to the colors is provided in appendix B.

A transition is observed from the smoke-laden air mass over Sumatra (areas 1 and 2 of Figs. 3 and 4) to less dense smoke at the west coast of Malaysia (area 3), and farther upwind to a smoke-free area on the east coast of Malaysia (area 4). Qualitatively, the transition in the cloud microstructure is evident in the changing of the coloration of the low-level clouds. The transition is more clearly seen in the T–r_e diagrams, where r_e increases gradually and the temperature of inferred glaciation decreases from the most polluted to the cleanest area, represented by Figs. 5a–d, respectively. According to Fig. 5d, the clouds over land near the upwind coast are more similar to the pristine maritime clouds (Fig. 2) than to the clouds growing in the smoke-plagued area (Figs. 5a,b). These results are consistent with the findings of Kaufman and Farser (1997), who retrieved r_e of clouds with tops warmer than 270 K over the Amazon basin to assess the impact of forest fire smoke on r_e. They showed that smoke typically reduced r_e from 15 to 9 μm.

4. Microphysical zones

4. Microphysical zones

Before examining more complex case studies, in which clouds undergo transition from maritime to

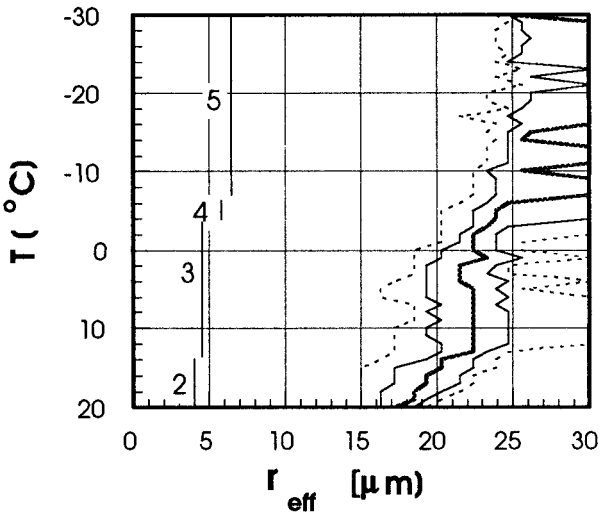

FIG. 2. Analysis of the temperature (T)–effective radius (r_e) relationship, for the clouds in the enclosed area plotted in Fig. 1. Plotted are the 10th, 25th, 50th, 75th, and 90th percentiles of the r_e for each 1°C interval. The median is indicated by the thick line. The vertical bars denote the vertical extent of the microphysical zones, as defined and numbered in section 4.

continental microstructure, it is helpful to develop some terminology. Based on the first two cases shown here, as well as on hundreds of other analyzed cases well distributed over the globe, the evolution of convective cloud-top microstructure as a function of T can be classified into the following five distinct vertical zones, not all necessarily appearing in a given cloud system.

1) *Diffusional droplet growth zone.* Very slow growth of cloud droplets with depth above cloud base, indicated by shallow slope of dr_e/dT.
2) *Droplet coalescence growth zone.* Large increase of the droplet growth rate dr_e/dT at T warmer than freezing temperatures, indicating rapid cloud-droplet growth with depth above cloud base. Such rapid growth can occur there only through drop coalescence.
3) *Rainout zone.* A zone where r_e remains stable between 20 and 25 μm, probably determined by the maximum drop size that can be sustained by rising air near cloud top, where the larger drops are precipitated to lower elevations and may eventually fall as rain from the cloud base. This zone is so named because droplet growth by coalescence is balanced by precipitation of the largest drops from cloud top. Therefore, the clouds seem to be raining out much of their water while growing. The radius of the drops that actually rain out from cloud tops is much larger than the indicated r_e of 20–25 μm, being at the upper end of the drop size distribution there.
4) *Mixed phase zone.* A zone of large indicated droplet growth rate, occurring at $T < 0$°C, due to coalescence as well as to mixed-phase precipitation formation processes. Therefore, the mixed-phase and the coalescence zones are ambiguous at the freezing temperatures. Because the first ice phase in growing continental clouds appears typically at $5° < -10$°C, the zones are arbitrarily separated at −10°C, except for the cases determined in the following discussion.
5) *Glaciated zone.* A nearly stable zone of r_e having a value greater than that of the rainout zone at below freezing temperatures, probably determined by the maximum ice particle size that can be sustained near cloud top, while the larger particles have been precipitated to lower elevations while aggregating and forming snowflakes.

There are two alternative ways to perceive the physical meaning of these zones. The first involves a description of the time evolution of a growing convective cloud top. The second involves a description of the vertical composition of a convective cloud at a given time throughout its depth. While the first alternative is always valid (under the assumption in section 2c), the second alternative can be valid only as long as no precipitation is falling through the cloud from higher levels. The presence of precipitation changes the microstructure of the cloud substances below the precipitation generating zone.

The diffusional droplet growth zone is well developed in continental clouds (Figs. 5a,b), but it is reduced in more maritime clouds (Fig. 5c) and vanishes in highly maritime clouds (Figs. 2 and 5d). In fact, cloud droplets start their growth diffusionally at the bases of all convective clouds; however, coalescence of highly maritime clouds starts within the depth required for clouds to pass the selection criterion for this method (i.e., visible reflectance of 40%).

The droplet coalescence growth zone is well developed a small distance above the bases of maritime clouds (Figs. 2 and 5d), but it appears higher in the cloud in less maritime clouds (Figs. 5b,c) and vanishes or overlaps with the mixed-phase zone in highly continental clouds (Fig. 5a).

The rainout zone can exist only in clouds with well-developed coalescence that have progressed to the

extent that a further increase of drop size is compensated for by the large drops falling from the cloud tops. Therefore the rainout zone exists just above the droplet coalescence growth zone. The rainout zone is well developed in maritime clouds (Fig. 2), but its extent is reduced in less maritime clouds (Fig. 5d) and completely vanishes in continental clouds (Figs. 5a–c).

The mixed-phase zone exists below the glaciated zone. Often the coalescence and mixed-phase zones overlap to one continuous area of rapid growth of r_e through the 0°C isotherm. In such cases the separation between the zones is set to −6°C (Fig. 5c), in accordance with aircraft observations in clouds with ample supercooled rain. The transition from the rainout zone to the glaciated zone. (Figs. 2 and 5d) is also defined as a mixed-phase zone. That transition is observed in the satellite analyses typically between −4° and −7°C.

A glaciated cloud is one for which practically all of its water has turned into ice particles. Cloud-top glaciation occurs at temperatures of about −5° to −10°C for clouds with well-developed rainout zones, typical of highly maritime clouds (Fig. 2), and in agreement with the laboratory experiments of Hallett and Mossop (1974). Glaciation occurs typically at about −15°C for less maritime clouds with coalescence (Fig. 5d), or colder for more continental clouds (Figs. 5a–c). Glaciation can occur at temperatures as cold as −30°C for extremely continental high-base clouds (not shown here).

All these classification criteria were translated into a computerized algorithm that is applied to user-specified windows in the satellite images on the work station screen. The examples shown here are the result of this algorithm.

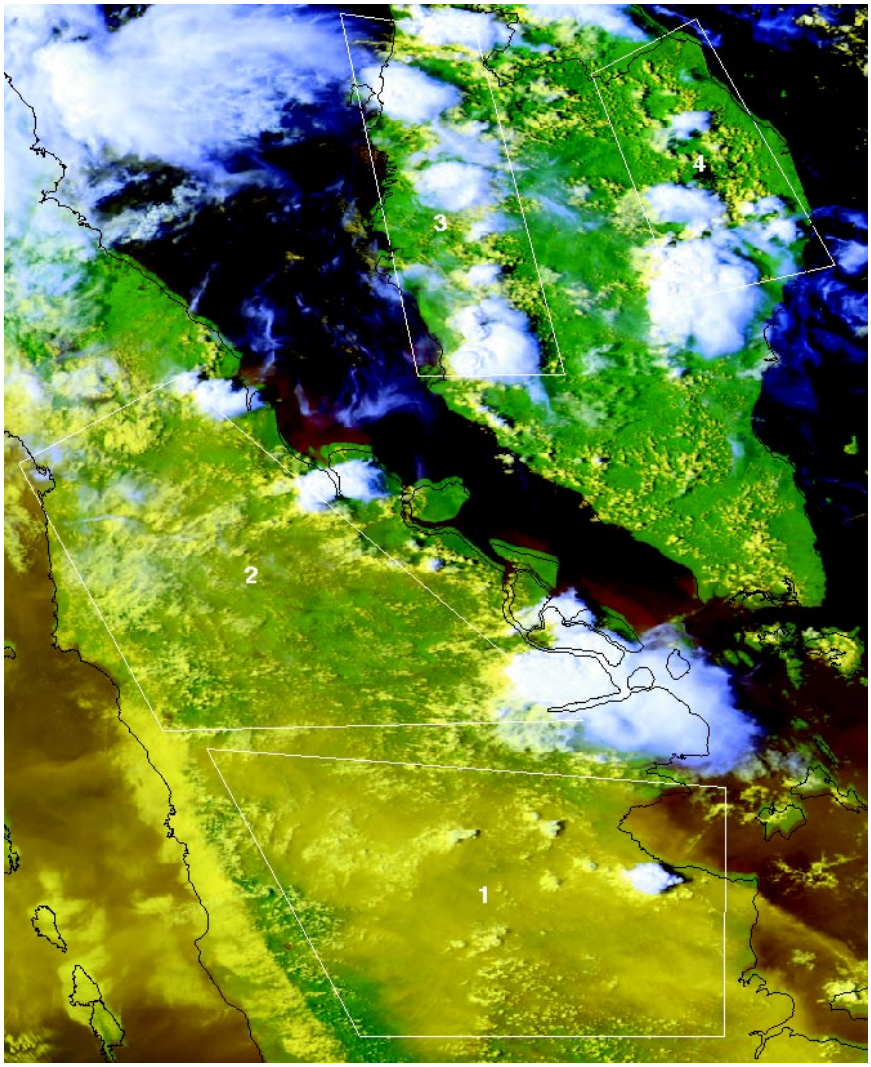

FIG. 3. A NOAA/AVHRR image from 14 October 1997 0732 UTC, of smoke and clouds in an area of about 600 × 1000 km over southern Malaysia and central Sumatra. The color is composed of red for visible reflectance, green for 0.9-μm reflectance, and blue for the inverse of the temperature. Ground is green, sea surface is dark, and the smoke appears as the fuzzy brown features over the sea background, or yellow fuzzy features over land, mostly over areas 1 and 2 over Sumatra. Smoke is less intense over western Malaysia (area 3). No smoke is seen over eastern Malaysia (area 4). Clouds are white and light blue for the cold tops and cirrus.

5. Case studies of transition from maritime to continental clouds

a. Transition from the eastern Mediterranean inland

After describing the extreme cases, and having developed the terminology, it is instructive to observe the other two situations where a maritime air mass moves from sea inland, while the clouds growing in it undergo transition from maritime to continental. These two cases were selected out of many possibili-

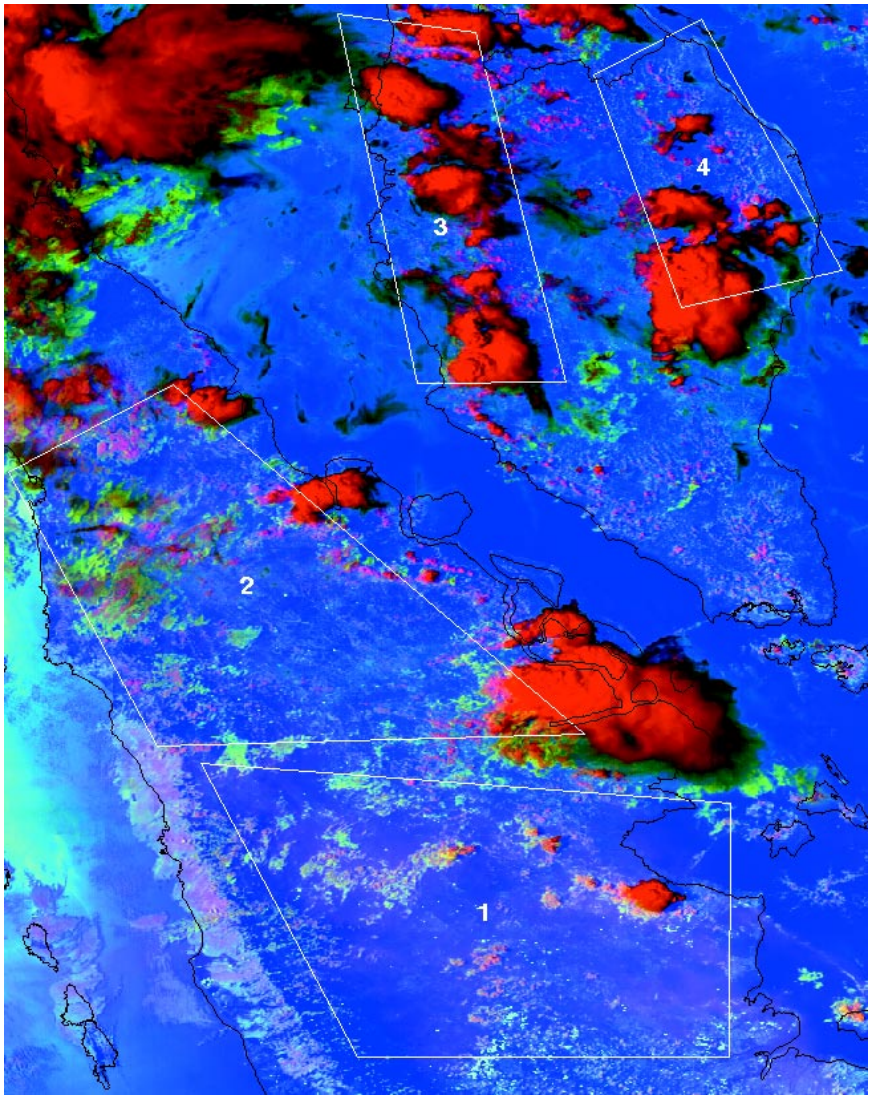

FIG. 4. A NOAA/AVHRR image from 14 October 1997 0732 UTC, of the same area shown in Fig. 3, but with color composed of red for visible reflectance, green for 3.7-μm reflectance (approximating r_e), and blue for the inverse of 10.8-μm brightness temperature. Cumulonimbus anvils appear as saturated red areas. Note the small less-developed clouds, changing their color from magenta and pink in the cleanest area (4) to more pink and white in the smoke-plagued areas (1 and 2). (See color palette in appendix A.)

ties as representing the "normal" situations that can be observed in most analyzed AVHRR images taken at random.

Figure 6 shows the changes of clouds in an air mass moving slowly from the eastern Mediterranean Sea (area 1) to Israel (area 2) and Jordan (area 3), while acquiring continental aerosols. The convection was triggered by surface heating. Therefore the convective clouds ingested the low-level aerosols, which affected their microphysical properties. The vertical extent of the clouds, as inferred from their temperature range, is similar for the three areas. The most developed cloud tops reached the −10°C level. There is a systematic color change of the convective cloud tops, ranging from red over sea, to orange over the coastal area, to yellow inland. The color change is produced by the increasing green component, interpreted as decreasing cloud-top particle size from sea inland. Quantitative estimation of this trend is provided in Fig. 7, which shows the T versus r_e relationships over the three framed areas. The cloud top (−10°C) median r_e is 19 μm over sea, 14 μm over the coast, and only 9 μm inland. Because convective clouds with $r_e > 14$ μm have been shown to produce precipitation (Rosenfeld and Gutman 1994), the clouds over sea are precipitating, while the clouds inland are not precipitating. The clouds over Israel were observed at that time to produce only a trace of precipitation.

b. Transition of trade wind clouds from the western Pacific inland

A similar case in a vastly different climatic regime is presented in Fig. 8. The viewed area shows the northern islands of the Philippines and the adjacent Pacific Ocean to the east. The area is under the influence of the northeast trade winds, which flow from the east coast inland, picking up continental aerosols on the way. Trade wind stratocumulus and cumulus clouds are scattered throughout the area. Orographic enhancement of the clouds is evident along the mountain ranges parallel to the east and west coasts of the northern island. A few isolated cumulonimbus clouds are evident by the saturated red color of their glaciated tops. Qualitative impression from the image (Fig. 8) shows that the coloration of the low-level clouds over the Pacific Ocean and the east coast is dominated by red shades, indicating the maritime nature of the clouds there. The red shades of the

clouds fade when they move inland toward the west coast of the islands, indicating the reduced cloud-top particle size as they incorporate more continental aerosols.

The quantitative analysis, given in Fig. 9, shows that clouds growing over the Pacific Ocean and the southwestern part of the island (area 1) are very maritime. This is evident by the deep rainout zone, shallow mixed-phase zone, and the warm glaciation temperature of –11°C.

Comparison of clouds over the east coast (area 2) to those inland and over the west coast (area 3) shows how the clouds lose their highly maritime nature inland. According to Figs. 9b and 9c, the median r_e is larger in area 2 than that of area 3 for any given T, reaching a plateau (r_e of 23 μm) at 12°C, suggesting that fully developed warm rain processes are reached at that temperature. This is depicted by the classification algorithm as the rainout

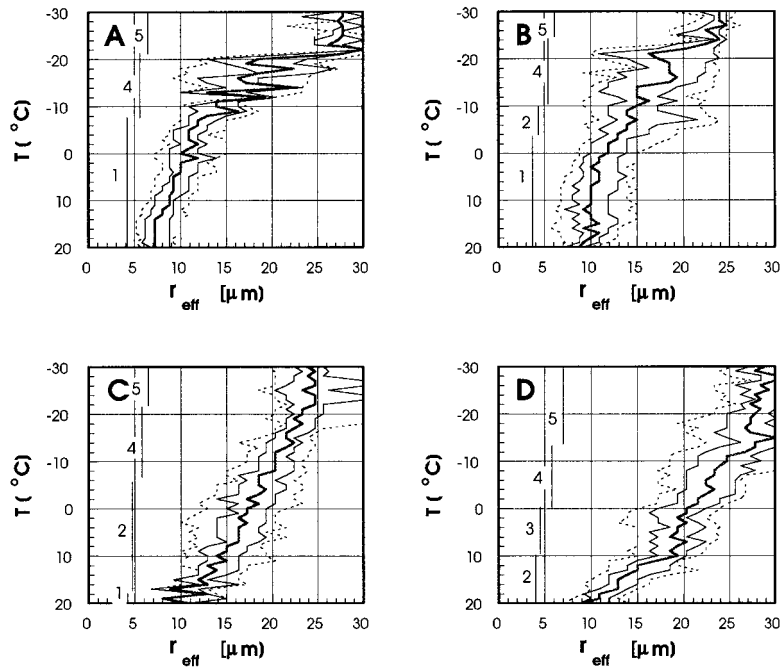

FIG. 5. Same as Fig. 2, but for the T vs r_e relations of clouds over Sumatra and Malaysia, for the four framed areas plotted in Figs. 3 and 4, where (a)–(d) are for areas 1–4, respectively.

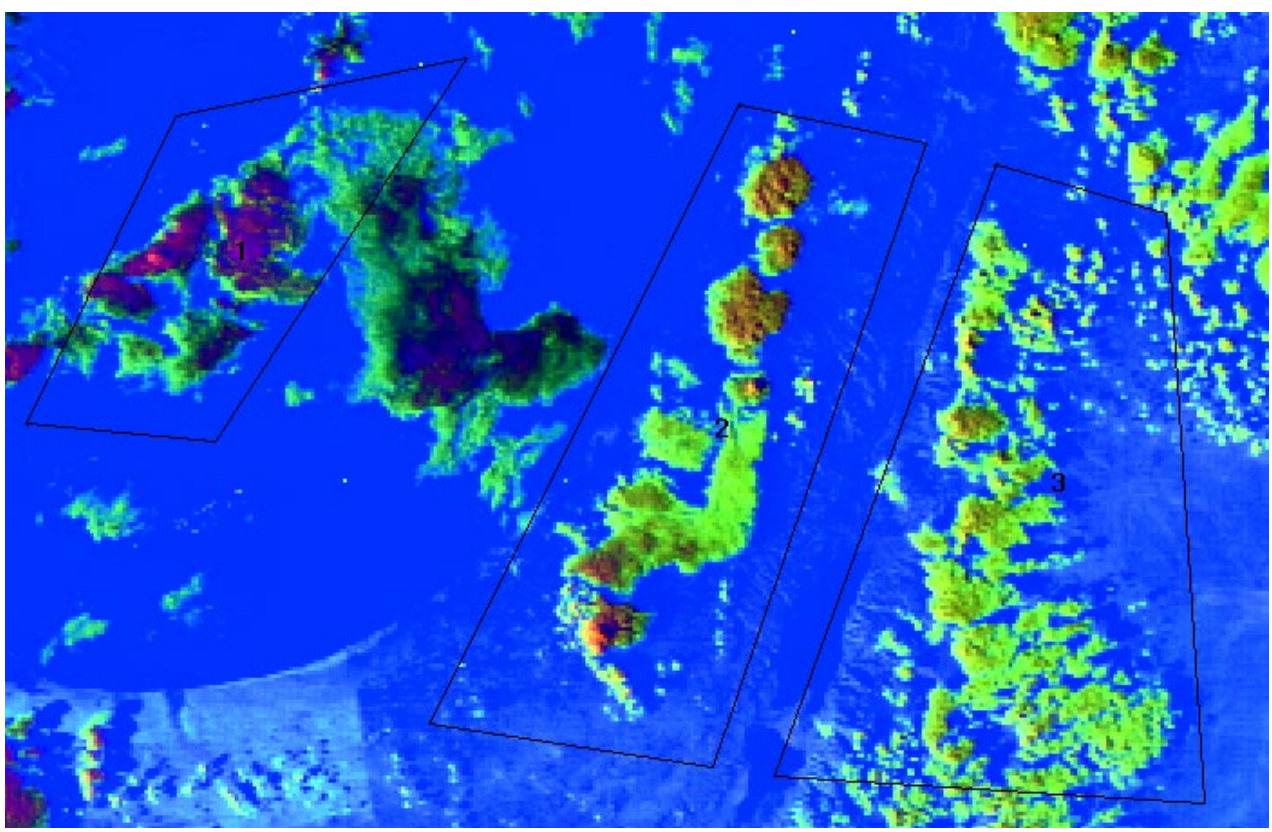

FIG. 6. As in Fig. 1, but for convective clouds developing in weak westerly flow from the Mediterranean Sea (area 1) to Israel (area 2) and Jordan (area 3) for an area of 400 × 240 km centered at 32.4°N, 31.5°E on 12 November 1992.

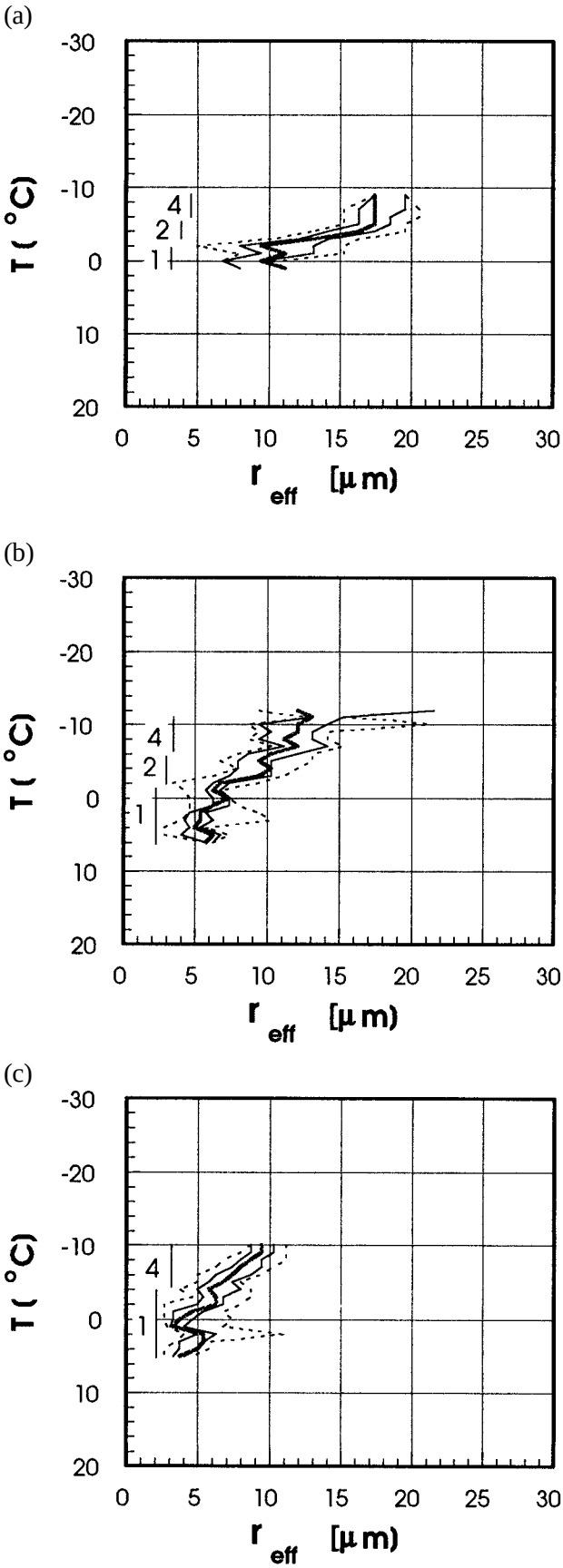

zone. The smaller r_e and lack of rainout zone in area 3 suggest that warm rain processes are slowed down in the inland clouds. The observation that $r_e > 14$ μm threshold in the inland clouds suggests that, although slowed down, warm rain is not completely suppressed there.

c. The impact of air pollution from a large city

Manila is a major metropolitan area with about 8 million people, producing urban air pollution at a sufficiently large scale (several tens of kilometers) so that its potential impact on clouds can be distinguishable by both the qualitative and quantitative schemes that are introduced here. We will now focus our attention, therefore, on the area of Manila and its vicinity. Fortunately, two small cumulonimbus clouds are formed, one in the ambient air to the north (area 4 of Fig. 8), and the other over the bay of Manila (area 5) downwind of the city. The T–r_e diagrams are quite noisy, due to the small sample size of cloudy pixels. However, a large difference between the two areas is still evident in Figs. 9d and 9e for the ambient air and the affected city areas, respectively.

The indicated microstructure of the warm portion ($T > 0$°C) of the clouds in area 4 (Fig. 9d) is closest to that of the clouds developing in area 3 (Fig. 9c), suggesting that the clouds there are similar to the clouds that have been modified by the continental aerosols inland, assuming continental tropical nature, with coalescence and some warm rain. In contrast, the coalescence in the clouds over Manila (Fig. 9e) is inferred to be strongly suppressed, as indicated by the extension of the diffusional growth zone up to the 0°C isotherm level. The microstructure of the clouds over Manila is more similar to that of the extremely continental clouds developing in the heavy forest fire smoke (Figs. 5a,b) than to the clouds developing in the ambient air near Manila.

6. Aircraft validation of the satellite retrievals and inferences

The previous sections showed the potential of multispectral, satellite-based remote sensing for the infer-

FIG. 7. Same as Fig. 2, but for the T vs r_e relations of clouds over the east Mediterranean for the three framed areas of Fig. 6, (a) for area 1, (b) for area 2, and (c) for area 3.

ence of the microstructure of convective clouds and their precipitation forming processes. Without validation, however, such inferences are merely an interesting curiosity. Accordingly, a major effort has been made to compare the satellite inferences of cloud properties with corresponding observations by aircraft and radar. The results of this data-validation effort to date are presented here; the validation effort is continuing.

a. Data sources

Cloud physics data for in situ validation were obtained from the following three projects:

1) the Israeli Rain Enhancement Project;
2) the Thai cloud physics aircraft, as part of the Thai rain enhancement project;
3) the Brief Assessment of the Affects of Smoke on Indonesian Clouds (BASIC) project in Indonesia during December 1997 (the same aircraft was used for Thailand and BASIC).

The instruments used are the following:

1) Forward Scattering Cloud-Droplet Spectrum Prober (FSSP) -100, measuring cloud drop size distribution within the range of 2–23 μm in drop radius;
2) hot-wire cloud liquid water, KING for Israel, droplet measuring technology for Thailand and Indonesia;
3) two-dimensional array imaging probe (2D-C) instrument, with nominal range size of 25–800 μm.

With respect to the 2D-C, it should be noted that the actual instrument minimum detectable size is larger than the maximum detectable size of the FSSP. It is manifested by the many observations of FSSP spectra with particles in the largest measurable bin but with no 2D-C measured particles, in spite of the much larger measurement volume of the 2D-C.

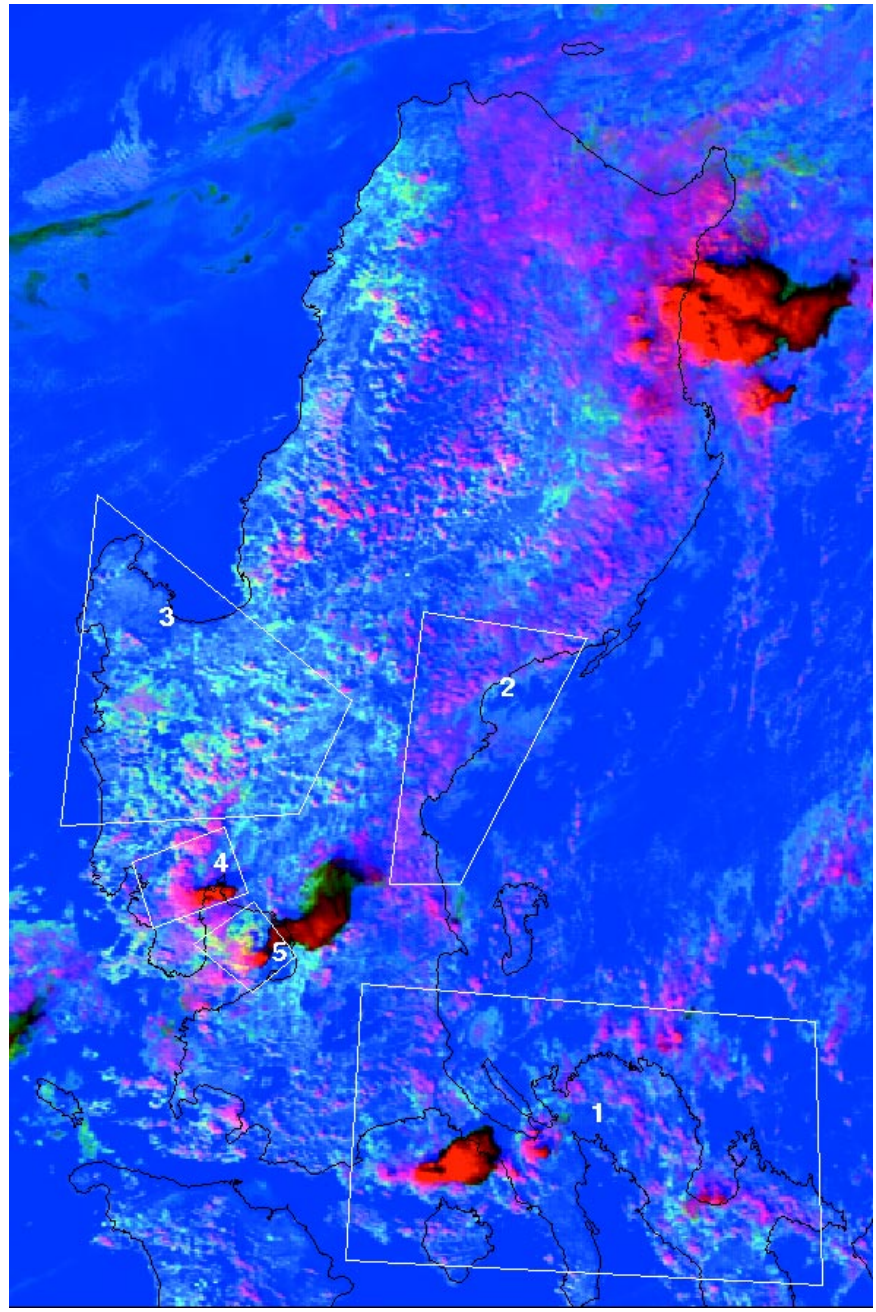

FIG. 8. As Fig. 1, but for a 400 × 650 km area over the northern half of the Philippines, on 14 December 1997 0623 UTC. The area is dominated by the NE trade winds, with maritime clouds, indicated by the pink and magenta colors (areas 1 and 2), moving inland and becoming more continental, as indicated by the fading of the red colors of the clouds (areas 3–5). The clouds in area 5, over the bay of Manila, are conspicuous by their white color, indicating that they are composed of very small particles.

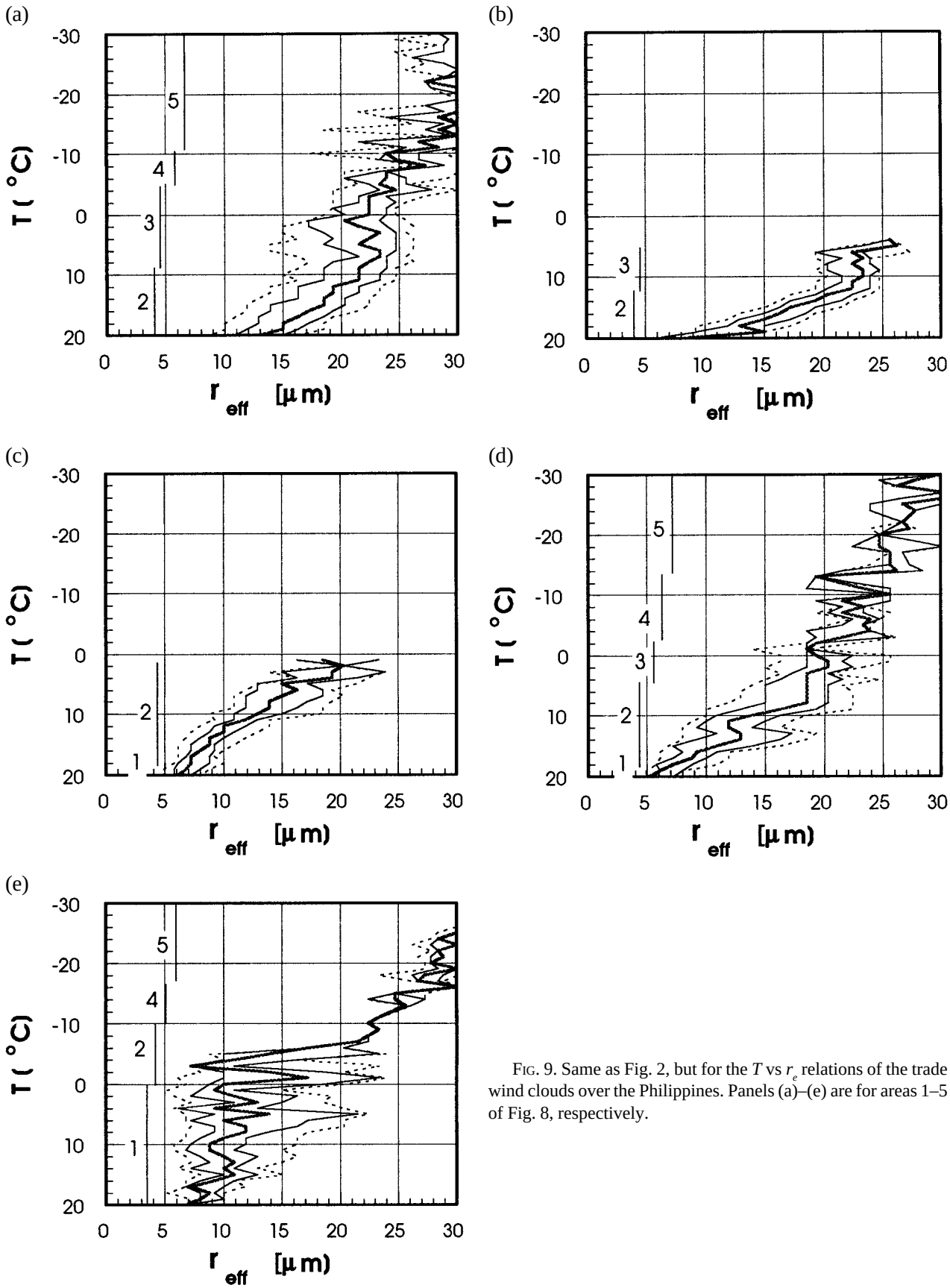

FIG. 9. Same as Fig. 2, but for the T vs r_e relations of the trade wind clouds over the Philippines. Panels (a)–(e) are for areas 1–5 of Fig. 8, respectively.

b. Validation of the assumption that r_e *is a conservative cloud property*

Two critical assumptions in the construction of the satellite retrieved T versus r_e are the following.

1) The cloud top r_e, observed by the satellite at a given time for a cloud ensemble, is similar to the evolution of r_e with height of a given cloud.
2) The r_e near cloud top is similar to that well within the cloud at the same height as long as precipitation does not fall through that cloud volume.

These assumptions were tested by conducting multiple aircraft penetrations at 3.5 km near and well below the tops of clouds at various stages of their development. The relationships between the cloud water content (g m^{-3}) and r_e and between cloud droplet concentration and r_e are provided in Figs. 10a and 10b, respectively, for measurements made on 18 December 1997, 1214–1304 local time (LT), over central Java, Indonesia. Each point represents the cloud properties integrated along 1 s of flight path. The bold points are from the most vigorous cloud, penetrated at 1254 LT about 1 km below its top. The circles are from a dissipating cloud penetrated at 1225 LT, grazing its top, with the sky partly visible during much of the penetration. The x's make up the balance of the sample.

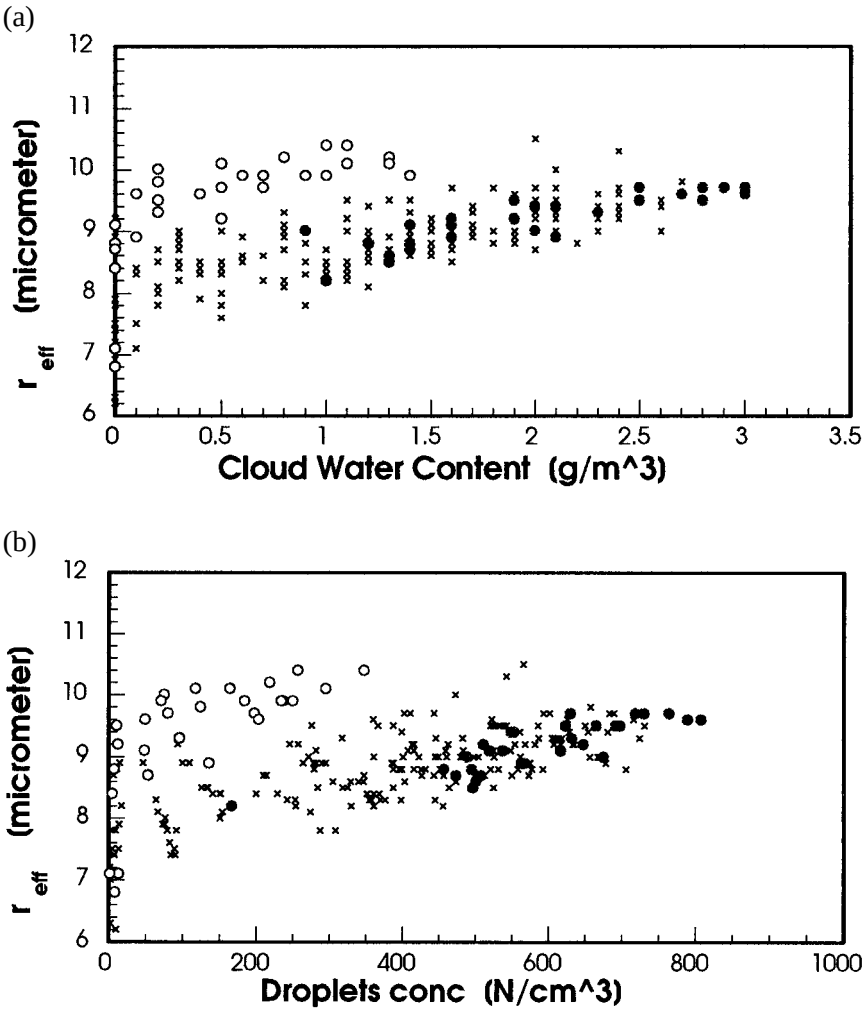

FIG. 10. (a) The relation between cloud-droplet water content (g m^{-3}) and r_e, for convective clouds at different stages of development at height of 3.5 km on 18 Dec 1997, 1214–1304 LT, over central Java, Indonesia. Each point represents the cloud properties integrated along 1 s of flight path. The bold points are from the most vigorous cloud, penetrated at 1254 LT about 1 km below its top. The circles are from a dissipating cloud penetrated at 1225 LT grazing its top, with the sky partly visible during much of the penetration. The x's make up the balance of the data. (b) The same as Fig. 3a, but for the relation between cloud droplet concentration (cm^{-3}) and r_e.

The amount of cloud liquid water content (CLWC) and the cloud droplet concentrations varied with cloud age, being maximal well inside the young vigorous clouds and minimal at the tops of decaying clouds. However, the cloud droplet r_e remained remarkably stable for both young and dissipating clouds within a narrow range of 2 μm for clouds having > 0.1 g m^{-3} of CLWC. This stability of r_e for a given cloud depth has been generally observed in all our research flights in cloud volumes that do not contain precipitation. Therefore, the cloud droplet r_e can be viewed as a conservative cloud property, being mainly a function of cloud depth for a given cloud condition, as long as precipitation has not developed in the cloud.

c. Validation case studies

The data for all case studies were analyzed similarly as follows.

The evolution with height of CLWC and droplet concentrations for convective cloud elements were documented and are shown in panel a of each case

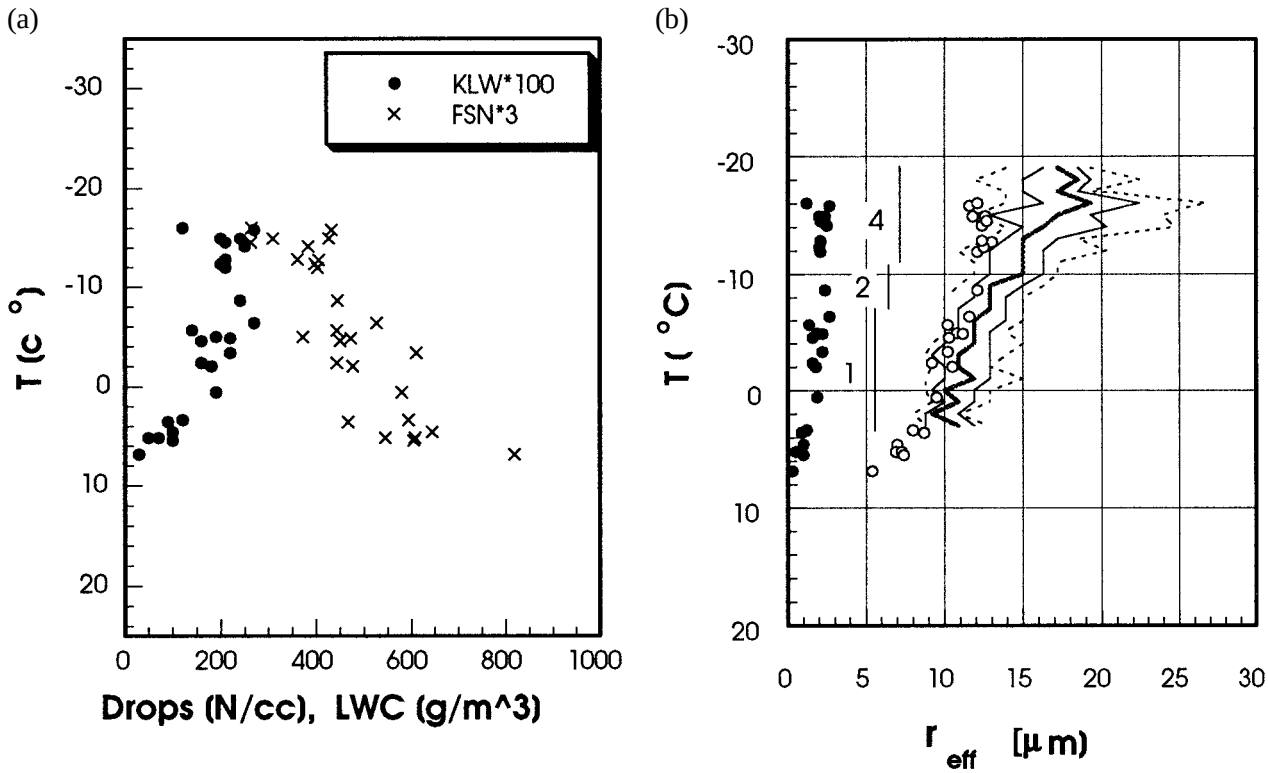

FIG. 11. First retrieval validation case, from Israel, 25 March 1995. (a) The aircraft-measured cloud liquid water contents (CLWC) and droplet number concentrations as a function of T; (b) the 10th, 25th, 50th, 75th, and 90th percentiles of the r_e for each 1°C interval. The median is indicated by the thick line. The vertical bars denote the different microphysical zones as numbered in the text. The aircraft FSSP r_e measurements are denoted as empty circles, and the CLWC (g m^{-3}) are in plotted black circles.

study. To bring all cases to a common scale, the height scale was converted to temperature. Because all cases involved convective clouds, the relation between height and cloud temperature is close to the moist-adiabatic lapse rate. Cloud water content should increase or remain near constant with height, and droplet concentrations should decrease slowly, as long as the clouds do not precipitate. The conversion of cloud droplets to precipitation at a given height is marked by a sharp decrease in the cloud droplet concentrations and water contents.

Upon applying these criteria to the first and second (Israeli) validation case studies (Figs. 11a and 12a), there is no indication for precipitation forming at $T > -10$°C and only weak evidence for it forming at $T < -10$°C in the first case (Fig. 11a). Indeed, the 2D-C instrument detected only a few dendritic ice crystals at $T = -12$°C, developing into graupel at the colder temperatures. The aircraft data of the second case did not exceed the −12°C level, because the clouds were visibly glaciating above that level, and the objective of that flight was to measure only clouds with supercooled water.

The evolution of satellite-retrieved effective radius (Sr_e) with height and the satellite-inferred microphysical zones are provided in panel b of each case study. The plots from the satellite data were generated as describe earlier for Figs. 2, 5, 7, and 9. The aircraft FSSP measurements of the effective droplet radius (Fr_e) are superimposed on the satellite diagrams as the small circles for direct comparison with the satellite measurements. The effective radii (r_e), calculated from the combined FSSP and 2D-C measurements (Cr_e) are denoted by triangles. Separation of the triangles from the circles is evidence for the existence of precipitation in the cloud. Note that Cr_e is not available for the Israeli case studies (Figs. 11b and 12b).

The aircraft data suggest that no warm rain formed in cases 1 and 2. According to the droplet concentrations, coalescence started to be active in case 1 above the −5°C level. No indication of coalescence is evident anywhere in case 2, as indicated by the relatively small decrease of cloud droplet concentrations with height. This is in agreement with the satellite-inferred diffusion zones for cases 1 and 2. The aircraft measurements (Fr_e) fell mostly between the median and lower

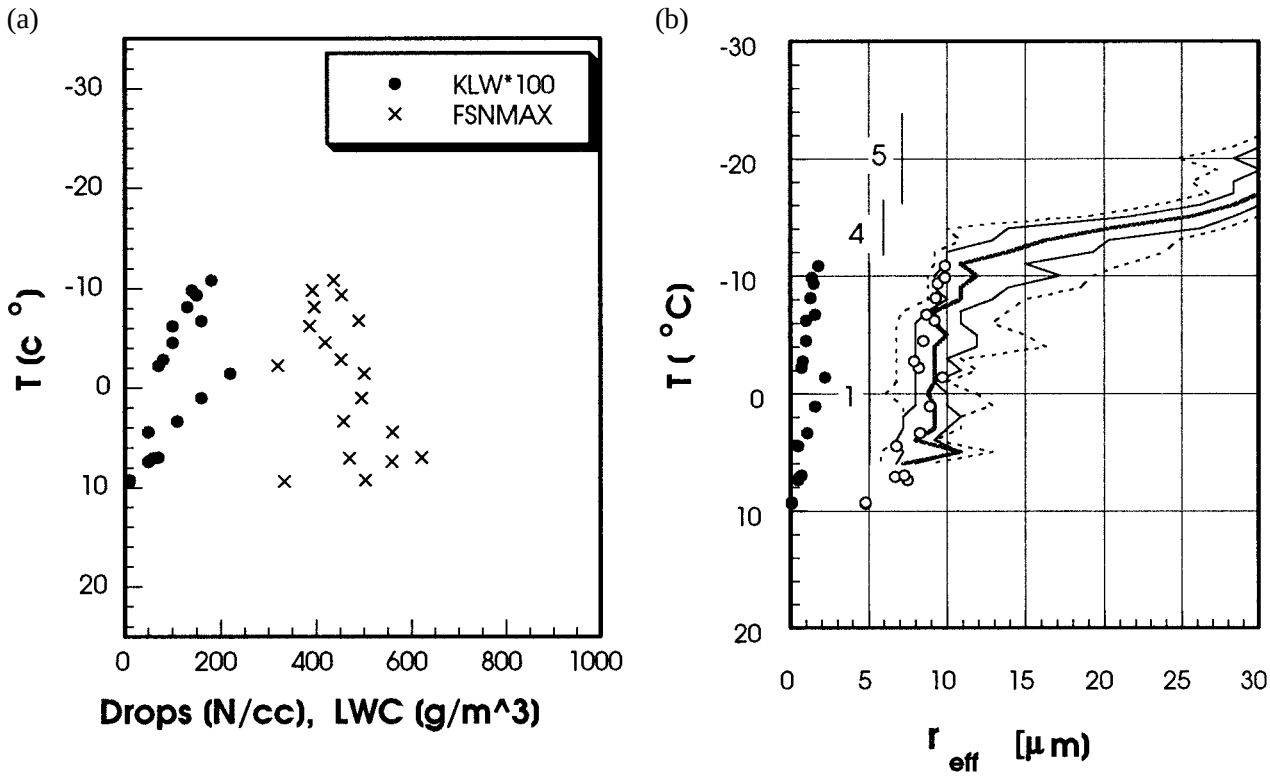

FIG. 12. As in Fig. 11, but for the second retrieval validation case, from Israel, 3 April 1995.

quartile of the satellite measurements (Sr_e) for the clouds in the diffusion and coalescence zones of cases 1 and 2.

In contrast to the highly microphysically continental clouds in Israel in cases 1 and 2, cases 3 and 4 (Figs. 13 and 14) are from the southeast Asian monsoon in northwest Thailand. The monsoon clouds had warm bases at about 20°C, with active coalescence starting a short distance above their bases and the production of raindrops detectable by the 2D-C at about the 12°C level.

In these two case studies the agreement between Sr_e and Fr_e is confined only to the warmest temperatures, below the level where much of the drop size distribution (DSD) is truncated by the limited range of the FSSP. The inclusion of the 2D-C in the calculation of the effective radius is very crude, and it still misses an important portion of the DSD, resulting in $Cr_e < Sr_e$ before larger drops have formed. Therefore, the Cr_e can be viewed only qualitatively, where $Cr_e - Fr_e$ serves as an indicator for the amount of precipitation. The Cr_e starts to deviate significantly from Fr_e at around an Sr_e of 15 μm, in agreement with the interpretation of that effective radius as the threshold for radar-detected precipitation (Rosenfeld and Gutman 1994). The steep decrease of the cloud droplet number concentration with height (Figs. 13a and 14a) is another means of validating the existence of coalescence and precipitation. Note that once there is coalescence and precipitation, Cr_e is > Sr_e.

Well-developed precipitation is indicated by $Cr_e >$ 30 μm, which is shown as a triangle on the right edge of the r_e scale of Figs. 13b and 14b. The satellite-inferred rainout zone (zone 3) coincides with these large Cr_e values. The large disparity between Sr_e and Cr_e values once precipitation has formed is explained by the fact that the satellite saturates at $r_e > 30$ μm whereas the 2D-C observes the larger drops.

The satellite-inferred mixed-phase zone (zone 4) starts near the level of −6°C, in agreement with the height at which supercooled rain was observed to start freezing in maturing convective elements. Note that in this zone there is continued decrease in the cloud water content and in the droplet number concentration.

In the glaciation zone the coldest temperature with aircraft measured CLWC > 0.3 was −23°C for case 3. An increase in the value of Sr_e is indicated at this temperature for this case. It seems that the zone definition algorithm defined as glaciated the cloud regions that contained large amount of ice precipitation even though some CLWC still existed in vigorous convective elements. This comparison suggests that the gla-

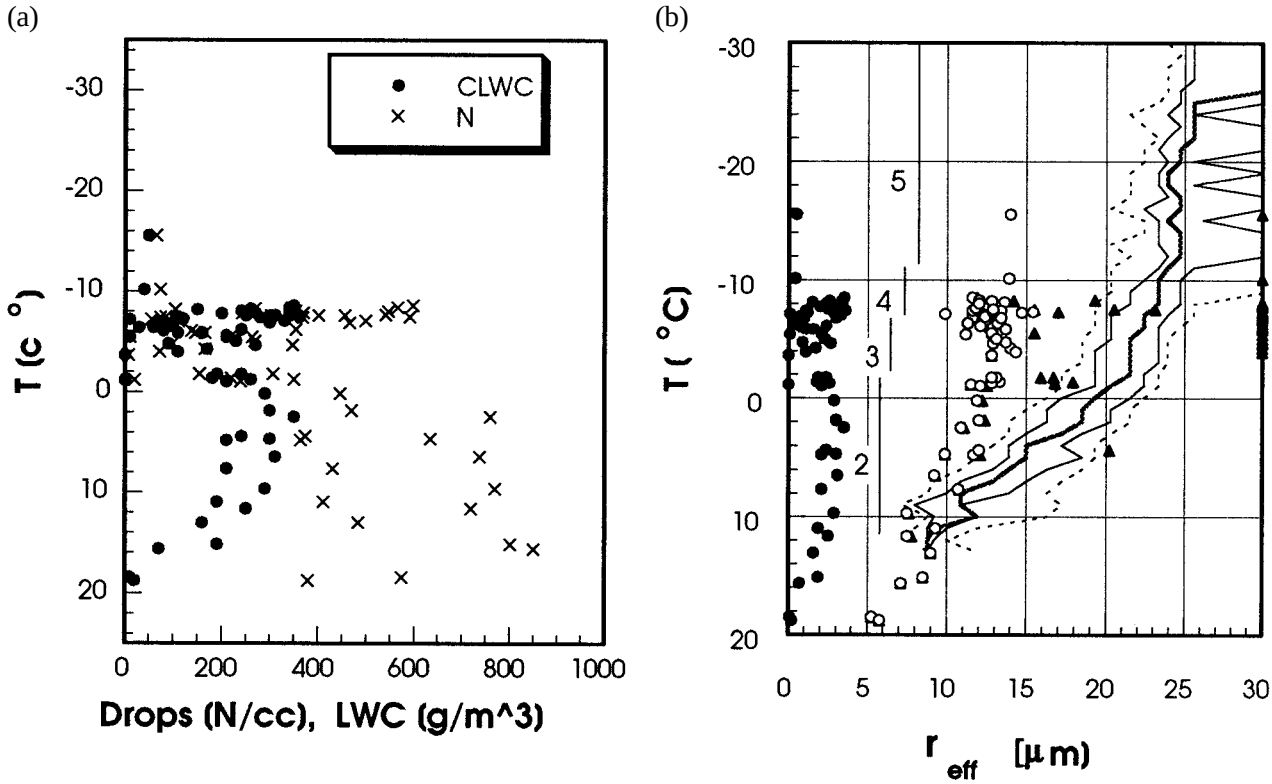

FIG. 13. As in Fig. 11, but for the third retrieval validation case, from Thailand, 29 June 1997. In addition, the r_e calculated from the combined FSSP and 2D-C aircraft measurements are plotted in the right panel as black triangles.

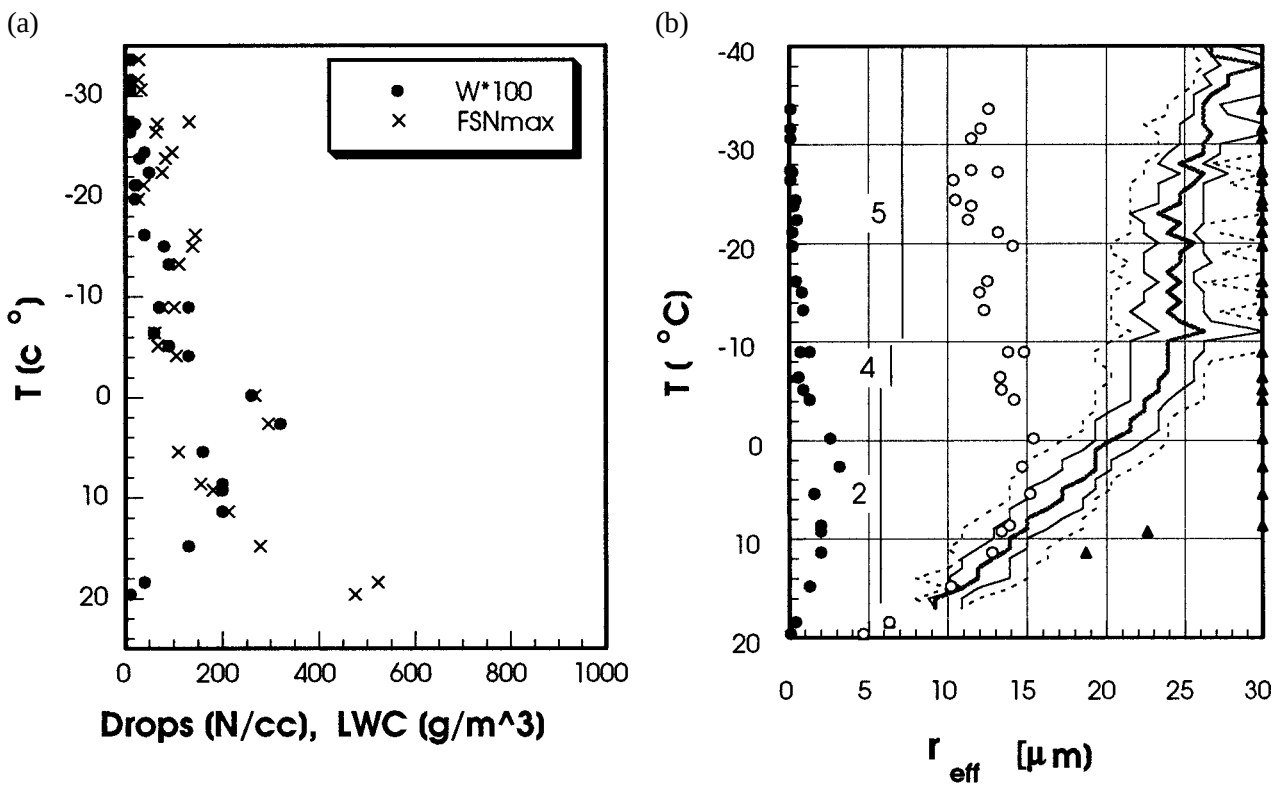

FIG. 14. As in Fig. 13, but for the fourth retrieval validation case, from Thailand, 16 July 1997.

ciation of the cloud droplets is indicated by yet another step in the T versus Sr_e function.

Several case studies had been obtained in Indonesia at the end of a period of extensive fires in the region. For purposes of illustration here the case on 18 December 1997 is selected for satellite retrieval and aircraft measurements in a region that appeared to be affected by some smoke advected from the dying fires (Fig. 15). Figures 10 and 11 are also based on this case study. Unlike the two Thai case studies, this Indonesian case has a rather deep diffusional growth zone to a temperature of about 8°C. The aircraft validation data show good agreement between Sr_e and Fr_e, which appears to be the rule rather than the exception in regions of diffusional droplet growth. Only scarce raindrops were observed, mainly in maturing clouds, by the 2D-C instrument down to 6°C. Further, the plot of the Sr_e suggests that no significant rain had formed in the cloud until the temperature was < 0°C.

7. Discussion and Summary

Multispectral analyses of satellite images have been used to infer the evolution of convective cloud particles and precipitation and these inferences have been compared favorably to aircraft validation data. Different microphysical processes from cloud base to top have been found to dominate, including zones of diffusional droplet growth, coalescence droplet growth, rainout, mixed-phase precipitation, and glaciation.

Large differences between convective clouds developing in maritime and continental clouds have been observed by this method. The droplet sizes of maritime clouds increases rapidly above cloud bases at a rate that implies the dominance of coalescence, while the droplet sizes of continental clouds increase much more slowly in agreement with theoretical calculations for diffusional growth. The coalescence zone is often observed in continental clouds, but at variable distance above their bases, just above the zone of diffusional growth. The depth of the diffusional growth zone is suggested as a measure of the "continentality" of the clouds, in line with Squires's (1958) classification.

Drops of maritime clouds continue growing by coalescence up to a maximum value, above which it appears that further growth is compensated for by precipitation of the larger drops from cloud top. This rainout mechanism is typical of maritime clouds with intense coalescence, but it is not observed in continen-

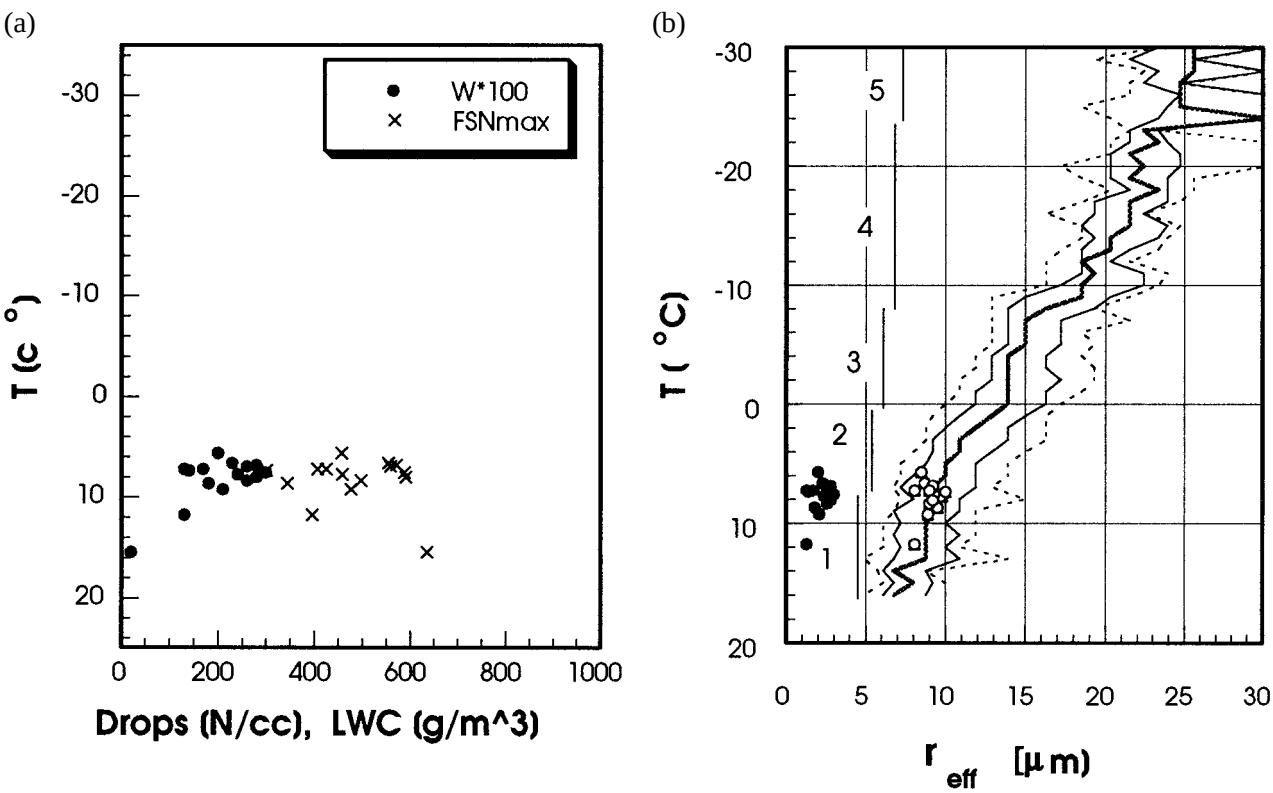

FIG. 15. As in Fig. 6, but for the fifth retrieval validation case, from Indonesia, 18 December 1997.

tal clouds with a deep diffusional growth zone above their bases. The inference of rainout in tropical maritime clouds is in agreement with the observations of Zipser and LeMone (1980), who showed that the Global Atmospheric Research Program (GARP) Atlantic Tropical Experiment convective clouds over the equatorial east Atlantic Ocean had low vertical velocities, too weak to lift raindrops through the freezing level.

Glaciation occurs in maritime clouds at much warmer temperatures (> −10°C) than continental clouds (−15° to −20°C, −30°C in extreme cases). Consequently, the indicated mixed-phase zone in maritime clouds is much shallower than in continental clouds. This inference is in agreement with the observations that maritime clouds have low supercooled liquid water contents that glaciate at temperatures > −10°C (Black and Hallett 1986), and weak updrafts and low radar reflectivities above the 0°C level (Zipser and Lutz 1994). The shallow mixed-phase zone and the depleted supercooled water due to the rainout process are also consistent with the observations that lightning frequency in maritime clouds is smaller by more than an order of magnitude than over the continents (Zipser 1994; Orville and Henderson 1986).

In all the observed cases of maritime air mass flowing inland, a gradual transition of the precipitation properties is observed from maritime to continental in a distance varying from few tens to several hundreds of kilometers. However, continental air that flows over sea does not seem to lose its continental properties so quickly (not shown here). This asymmetry suggests that pollution of a clean maritime air mass is much faster than its return to pristine conditions.

According to the 14-μm precipitation threshold criterion (Rosenfeld and Gutman 1994), the cloud systems over Malaysia and Indonesia (Figs. 3, 4, and 5), the Mediterranean (Figs. 6 and 7), and the Philippines (Figs. 8 and 9) were undergoing a transition from precipitating maritime clouds to less efficient or nonprecipitating continental clouds. This is consistent with the traditional microphysical classification of clouds forming in air masses with maritime or continental CCN aerosols (Squires 1958). Although this type of transition is quite common, this may be the first time that it has been observed on the synoptic scale.

It is important to note that cloud microstructure and precipitation-forming processes were found to be sensitive to pollution added to the background of an already continental air mass. This situation is in contrast to the diminished susceptibility of cloud albedo to added aerosols in continental air mass and thick clouds (Platnick and Twomey 1994). It follows that natural and anthropogenic aerosols can substantially modify clouds not only in pristine environments, as has already been demonstrated by the ship tracks, but they can also have a profound impact on cloud microstructure and precipitation in continental environments, leading to substantial weather modification in populated areas. The case study over Manila, presented here in Figs. 9c and 9d, is a case in point.

The interactions between aerosols and clouds affect precipitation and play a major role in the energy budget of the earth (Hobbs 1993). These processes are recognized as the least-known component of the climate system and can potentially determine the magnitude of global climate change (Houghton et al. 1994). The results presented here may be the first time that the interactions between the aerosols and clouds and the effect of these interactions on precipitation have been viewed on a large scale from space. These new capabilities have produced findings that are critical to the understanding of the role that aerosols play in determining the composition of clouds, their precipitation, and even their electrical activity. They have paved the way for more extensive climatological research that will make use of satellite data and new analysis techniques along with radar and aircraft observations of precipitation, cloud properties, and aerosols.

Acknowledgments. This research was funded partially by the U.S.–Israel Binational Science Foundation. The authors thank Dr. W. Woodley for his helpful suggestions in the writing of the manuscript. The authors are grateful to Dr. Garik Gutman from NOAA/NESDIS and Dr. Surat from the Asian Institute of Technology for providing the satellite data for this study. The authors thank Drs. T. Nakajima and M. King for the use of their radiative transfer model in this study. Special thanks are due to the Israeli Rain Enhancement Branch of Electrical Mechanical Services for providing the research aircraft for measurements in clouds over Israel, and to the Thailand Bureau of Royal Rainmaking and Agricultural Aviation, Ministry of Agriculture and Cooperatives, for providing the research aircraft and cloud physics data over Thailand and Indonesia. Thanks are due to Dr. Roelof Bruintjes from NCAR, who led the field campaign of Brief Assessment of the Affects of Smoke on Indonesian Clouds (BASIC).

Appendix A: Color pallets for the composite images in Figs. 1, 4, 6, and 8

The four pallets at the top of the following page pertain to four discrete values of temperature (blue) specified at the top of each pallet, and for all possible combinations of visible reflectance (red) specified on

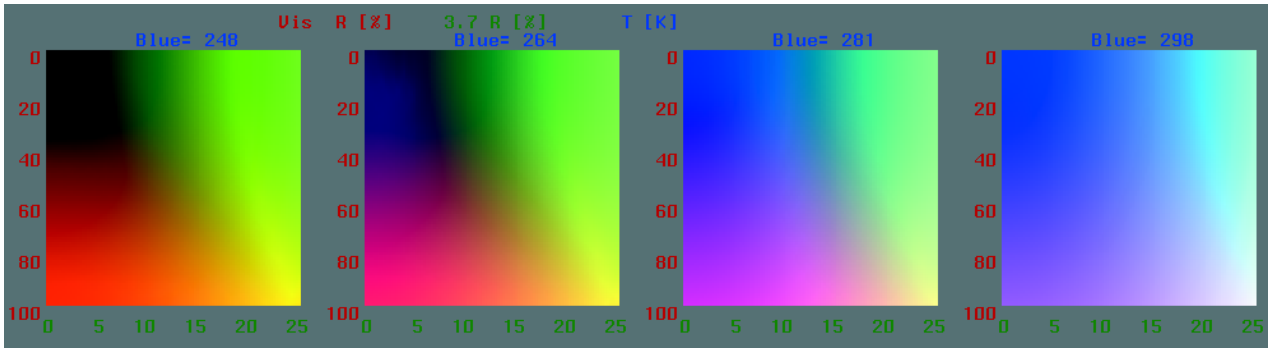

the ordinate (%), and 3.7-μm reflectance (green) specified on the abscissa (%). The colors intensity varies from 0% to 100% for the colors as follows.

Red: 0%–100% of visible reflectance.
Green: 0%–25% of 3.7-μm reflectance.
Blue: 248–298 K of cloud-top or surface temperature.

Appendix B: The red-green-blue color compositions and their interpretation

Appendix B: The red-green-blue colors compositions and their interpretation

color components

Redder: Larger visible reflectance
Greener: Smaller cloud top particles
Bluer: Warmer tops

color compositions

White: Low thick water or dust clouds, no precipitation.
- High red 100%: Bright and thick clouds.
- High green 25%: Small particles.
- High blue: 281K: Warm tops.

Red: Deep precipitating clouds (precipitation not necessarily reaching the ground)
- High red 100%: Bright and thick clouds.
- Low green 0%: Large particles.
- Low blue 248K: Very cold tops.

Yellow: Supercooled thick water clouds
- High red 100%: Bright and thick clouds.
- High green 25%: Small particles.
- Low blue 264K: Cold tops.

Green: Supercooled water or small ice particles thin clouds, typically altocumulus, altostratus and tropical cirrus
- Low red 30%: Thin clouds on dark surface background.
- High green 20%: Small particles.
- Low blue 248K: Very cold tops.

Black: Large ice particles, thin clouds, often cirrus composed of large particles.
- Low red 20%: Dark and thin clouds.
- Low green 0%: Large particles.
- Low blue: 248K: Very Cold tops.

Dark magenta: Warm rain clouds.
- Medium red 60%: Bright and moderately thick clouds.
- Low green 3%: Large particles.
- High blue 281K: Warm tops.

Magenta : "Warm ice" precipitating clouds, or snow on the ground.
- High red 80%: Bright and thick clouds.
- Low green 0%: Large particles.
- Medium blue 264K: Mild tops (0 to -10°C).

Blue: Surface
- Low red 10%: Low visible reflectance surface.
- Low green 5%: Low mid IR reflectance surface.
- High blue: 298: Warm surface.

Arakawa, A., and W. H. Schubert, 1974: Interaction of cumulus cloud ensemble with the large-scale environment. Part I. *J. Atmos. Sci.*, **31,** 671–701.

Black, R. A., and J. Hallett, 1986: Observations of the distribution of ice in hurricanes. *J. Atmos. Sci.*, **43,** 802–822.

Coakley, J. A., R. L. Bernstein, and P. R. Durkee, 1987: Effects of ship-stack effluents on cloud reflectivity. *Science*, **237,** 1020–1022.

Eck, T. F., and B. N. Holben, 1994: AVHRR split window temperature differences and total precipitable water over land surfaces. *Int. J. Remote Sens.*, **15,** 576–582.

Hallett, J., and S. C. Mossop, 1974: Production of secondary ice particles during the riming process. *Nature*, **249,** 26–28.

Hobbs, P. V., 1993: *Aerosol–Cloud–Climate Interactions.* Academic Press, 233 pp.

Houghton, J. T., L. G. Meira Filho, J. Bruce, H. Lee, B. A. Callander, E. Haites, N. Harris, and K. Maskell, Eds., 1994: *Climate Change 1994—Radiative Forcing of Climate Change and an Evaluation of the IPCC IS92 Emission Scenarios. Reports of Working Groups I and II of the Intergovernmental Panel on Climate Change.* Cambridge University Press, 339 pp.

Jorgensen, D. P., and M. A. LeMone, 1989: Vertical velocity characteristics of oceanic convection. *J. Atmos. Sci.*, **46,** 621–640.

Kaufman, Y. J., and T. Nakajima, 1993: Effect of Amazon smoke on cloud microphysics and albedo—Analysis from satellite imagery. *J. Appl. Meteor.*, **32,** 729–744.

——, and R. S. Farser, 1997: The effect of smoke particles on clouds and climate forcing. *Science*, **277,** 1636–1639.

Lensky, M. I., and D. Rosenfeld, 1997: Estimations of precipitation area and rain intensity based on the microphysical properties retrieved from NOAA AVHRR data. *J. Appl. Meteor.*, **36,** 234–242.

Nakajima, T., and M. D. King, 1990: Determination of the optical thickness and effective particle radius of clouds from reflected solar radiation measurements. Part I: Theory. *J. Atmos. Sci.*, **47,** 1878–1893.

Orville, R. E., and D. Henderson, 1986: Global distribution of midnight lightning: September 1977 to August 1978. *Mon. Wea. Rev.*, **114,** 2640–2653.

Platnick, S., and S. Twomey, 1994: Remote sensing the susceptibility of cloud albedo to changes in drop concentration. *J. Atmos. Res.*, **34,** 85–98.

Radke, L. F., J. A. Coakley, and M. D. King, 1989: Direct and remote sensing observations of the effects of ships on clouds. *Science*, **246,** 1146–1149.

Rosenfeld, D., and G. Gutman, 1994: Retrieving microphysical properties near the tops of potential rain clouds by multispectral analysis of AVHRR data. *J. Atmos. Res.*, **34,** 259–283.

Squires, P., 1958: The microstructure and colloidal stability of warm clouds. *Tellus*, **10,** 256–271.

Zipser, E. J., 1994: Deep cumulonimbus cloud systems in the Tropics with and without lightning. *Mon. Wea. Rev.*, **122,** 1837–1851.

——, and M. A. LeMone, 1980: Cumulonimbus vertical velocity events in GATE. Part II: Synthesis and model core structure. *J. Atmos. Sci.*, **37,** 2458–2469.

——, and K. Lutz, 1994: The vertical profile of radar reflectivity of convective cells: A strong indicator of storm intensity and lightning probability? *Mon. Wea. Rev.*, **122,** 1751–1759.